

Off-diagonal magnetoimpedance in field-annealed Co-based amorphous ribbons

N. A. Buznikov,^{a)} CheolGi Kim,^{b)} Chong-Oh Kim, Seok-Soo Yoon,^{c)} and Lan Jin

*Research Center for Advanced Magnetic Materials, Chungnam National University,
Daejeon 305-764, Korea*

Abstract

The off-diagonal magnetoimpedance in field-annealed CoFeSiB amorphous ribbons was measured in the low-frequency range using a pick-up coil wound around the sample. The asymmetric two-peak behavior of the field dependence of the off-diagonal impedance was observed. The asymmetry is attributed to the formation of a hard magnetic crystalline phase at the ribbon surface. The experimental results are interpreted in terms of the surface impedance tensor. It is assumed that the ribbon consists of an inner amorphous region and surface crystalline layers. The coupling between the crystalline and amorphous phases is described through an effective bias field. A qualitative agreement between the calculated dependences and experimental data is demonstrated. The results obtained may be useful for development of weak magnetic-field sensors.

PACS numbers: 72.15.Gd; 75.50Kj; 75.60.Ej; 75.60Nt

^{a)} Permanent address: Institute for Theoretical and Applied Electrodynamics,
Russian Academy of Sciences, Moscow, Russia

^{b)} Author to whom correspondence should be addressed; electronic mail: cgkim@cnu.ac.kr

^{c)} Permanent address: Department of Physics, Andong National University, Andong, Korea

I. INTRODUCTION

The giant magnetoimpedance (GMI) effect consists of a huge change in the impedance of a soft magnetic conductor in the presence of a static magnetic field. The interest in the GMI is supported by possible use of the effect in various technological applications, in particular, for the development of weak magnetic-field sensors. The linearity and the sensitivity for the magnetic field are the most important parameters in practical applications of the GMI effect. To improve the linear characteristic of the GMI response, the asymmetric GMI is very promising.^{1,2}

There are several mechanisms of the asymmetric GMI,¹ one of these has been observed in Co-based amorphous ribbons annealed in air in the presence of a weak magnetic field.^{3–6} The asymmetry of the GMI profile has been ascribed to the formation of a hard magnetic phase due to the surface crystallization of an amorphous ribbon.^{4,5} The coupling between the crystalline and amorphous phases produces an effective bias field that is responsible for the asymmetric GMI in field-annealed ribbons.^{3,6} At sufficiently low frequencies, the GMI profile exhibits a drastic steplike change in the impedance near zero field (so called “GMI valve”), and at high frequencies, the field dependence of the impedance shows asymmetric two-peak behavior.⁶

Usually, the GMI is measured as the voltage across a soft magnetic sample. Another method to detect the field-dependent signal consists of the use of the pick-up coil wound around a sample. This method is based on the cross-magnetization process, which appears since the current induces an ac axial magnetization variation and, hence, the pick-up coil voltage. The effect has been referred to as the off-diagonal magnetoimpedance. The off-diagonal magnetoimpedance has been studied in detail for Co-based amorphous wires^{7–12} and multi-layered films.^{13,14} It has been demonstrated that the off-diagonal magnetoimpedance may be preferable for sensor applications since it generates a linear voltage response with enhanced field sensitivity. However, up to now the effect has not been investigated in amorphous ribbons.

In this paper, we present a study of the off-diagonal magnetoimpedance in field-annealed Co-based amorphous ribbons within the frequency range 0.1–1 MHz. The

asymmetric two-peak behavior of the field dependence of the off-diagonal impedance was observed, which is related to the coupling between crystalline and amorphous phases. The experimental results are interpreted in terms of the field and frequency dependent surface impedance tensor.^{2,8,11,15,16} It is assumed that the ribbon consists of an inner amorphous core and two outer crystalline layers. Neglecting a domain structure, the off-diagonal magnetoimpedance is calculated. A satisfactory agreement between the calculated field and frequency dependences of the off-diagonal impedance and experimental data is demonstrated.

II. EXPERIMENT

Amorphous ribbons $\text{Co}_{66}\text{Fe}_4\text{Si}_{15}\text{B}_{15}$ were prepared by the rapid solidification technique. The ribbons were annealed in air at a temperature of 380 °C during 8 h. A field of 3 Oe was applied along the sample axis during the annealing. The width of the samples was 2 mm, and their thickness was 20 μm . For experiments, the ribbons of length 3 cm were used.

The schematic diagram of the experimental setup is shown in Fig. 1. The amplitude I_0 of the ac current was controlled to 1 mA by a resistor of 100Ω connected with the sample in series, and the current frequency f was varied from 0.1 to 1 MHz by a function generator. The longitudinal dc magnetic field H_e created by a Helmholtz coil was changed from -40 to 40 Oe. The pick-up coil was wound around the ribbon. The pick-up coil had 25 turns and was 5.5 mm in length. In the experiments, the amplitude V_c of the voltage induced in the pick-up coil was measured by a lock-in amplifier as a function of the frequency and longitudinal dc magnetic field. From the measured voltage amplitude, the off-diagonal impedance Z_c was calculated as $Z_c = V_c/I_0$.

III. RESULTS AND DISCUSSION

Figure 2 presents the measured field dependence of the off-diagonal impedance at different frequencies. The dependence exhibits asymmetric two-peak behavior, with the peak at a positive field being higher than the peak at a negative field. Note that the direction of the positive field coincides with that of the annealing field. Similar to the case of the GMI response measured as the voltage across the field-annealed ribbons,³⁻⁶ the asymmetry in the

field dependence of the off-diagonal impedance may be attributed to the coupling between the amorphous phase and the surface crystalline layers appearing after annealing.

It follows from Fig. 2 that there is a hysteresis in the field dependence of the off-diagonal impedance for increasing and decreasing fields. The hysteresis was observed within the region of low external fields and may be related to the effect of the domain structure. It is seen from Fig. 2 that the off-diagonal magnetoimpedance increases with the frequency, and, in the same time, the asymmetry between peaks decreases. The field dependence of the off-diagonal impedance at low magnetic fields demonstrates almost linear behavior, which is promising for sensor applications. At $H_e=0$, the field sensitivity $\Delta Z_c/\Delta H_e$ attains $0.02 \Omega/\text{Oe}$, $0.05 \Omega/\text{Oe}$, and $0.14 \Omega/\text{Oe}$ for 100 kHz , 500 kHz , and 1 MHz , respectively.

To interpret the observed dependences of the off-diagonal impedance we use a simple model, which allows one to describe main features of the experimental results. The annealing leads to the crystallization of the surface layers of the ribbon.⁴ Due to the presence of the annealing field, the crystallites are magnetically ordered, which results in an effective unidirectional surface anisotropy. The value of the unidirectional anisotropy field H_u is sufficiently high and attains several hundreds of Oe.⁶ In this analysis, we consider the ribbon of thickness t consisting of an inner amorphous region and two outer crystalline layers at the ribbon surface.¹⁷ It is assumed also that the surface layers have different thickness, t_1 and t_2 . The difference in the thickness of the crystalline layers may be related to peculiarities of the field-annealing process. During the annealing, one side of the ribbon is located on the substrate, which may result in the change of the crystalline layer thickness in comparison with that at another side of the ribbon. It is assumed further that the unidirectional anisotropy field in the outer layers has the constant angle φ with respect to the transverse direction (a sketch of the coordinate system is shown in Fig. 3). Note that the direction of H_u differs from that of the annealing field, which may be attributed to the influence of the amorphous core on the crystallization process in the surface layers.^{17,18}

The distribution of the magnetization in the amorphous core depends on the stresses induced in the ribbon during the fabrication process and may vary significantly over the ribbon volume. We assume for simplicity that the amorphous core has a single-domain

structure, the uniaxial anisotropy field H_a is constant, and the anisotropy axis makes the angle ψ with the transverse direction in the whole amorphous region. The coupling between amorphous and crystalline phases induces the effective bias field H_b in the amorphous region, with the bias field being in the opposite direction to the unidirectional anisotropy field H_u ⁶ (the angle of the bias field with respect to the transverse direction is $\varphi+\pi$, see Fig. 3). We assume for simplicity that the effective bias field does not vary over the amorphous region.

The analysis is concerned with the calculation of the surface impedance tensor,^{2,8,11,15,16} which relates the components of the electric and magnetic field at the sample surface. The surface impedance calculation is based on a solution of Maxwell equations for the electric and magnetic fields together with the Landau–Lifshitz equation. The permeability tensor for both the inner amorphous region and outer crystalline layers can be found by means of the well-known procedure of the solution of the linearized Landau–Lifshitz equation, and the permeability is represented by a nondiagonal tensor.^{2,8,10,11}

Since the ribbon length and width are much higher than its thickness, we may assume that the fields depend only on the coordinate perpendicular to the ribbon plane (x -coordinate). In this case, Maxwell equations in the amorphous region, $-t/2+t_2 < x < t/2-t_1$, reduce to coupled differential equations for the transverse, $h_y^{(a)}$, and longitudinal, $h_z^{(a)}$, components of the ac magnetic field:^{9,13}

$$\begin{aligned} \frac{d^2 h_y^{(a)}}{dx^2} + \frac{2i}{\delta_0^2} (1 + \mu_1 \sin^2 \theta) h_y^{(a)} &= \frac{2i}{\delta_0^2} \mu_1 h_z^{(a)} \sin \theta \cos \theta, \\ \frac{d^2 h_z^{(a)}}{dx^2} + \frac{2i}{\delta_0^2} (1 + \mu_1 \cos^2 \theta) h_z^{(a)} &= \frac{2i}{\delta_0^2} \mu_1 h_y^{(a)} \sin \theta \cos \theta, \end{aligned} \quad (1)$$

where $\delta_0 = c/(2\pi\sigma\omega)^{1/2}$ is the skin depth in nonmagnetic material, c is the velocity of light, σ is the ribbon conductivity, $\omega = 2\pi f$ is the angular current frequency, and μ_1 is the effective permeability of the amorphous region, which is given by

$$\begin{aligned} \mu_1 &= \frac{\omega_m(\omega_m + \omega_1 - i\kappa\omega)}{(\omega_m + \omega_1 - i\kappa\omega)(\omega_2 - i\kappa\omega) - \omega^2}, \\ \omega_m &= \gamma 4\pi M, \\ \omega_1 &= \gamma [H_a \cos^2(\theta - \psi) - H_b \cos(\theta - \varphi) + H_e \sin \theta], \\ \omega_2 &= \gamma [H_a \cos\{2(\theta - \psi)\} - H_b \cos(\theta - \varphi) + H_e \sin \theta]. \end{aligned} \quad (2)$$

Here M is the saturation magnetization, γ is the gyromagnetic constant, κ is the Gilbert damping parameter, and θ is the equilibrium angle between the magnetization vector and the transverse direction. The angle θ can be found by minimizing the free energy, which can be presented as a sum of the uniaxial anisotropy energy, the bias field energy, and the Zeeman energy. The minimization procedure results in the following equation for the equilibrium angle:¹⁷

$$H_a \sin(\theta - \psi) \cos(\theta - \psi) - H_b \sin(\theta - \varphi) - H_e \cos \theta = 0. \quad (3)$$

Since the unidirectional anisotropy field H_u in the crystalline layers is high, we may assume that the direction of the magnetization in the surface layers is almost independent of the external field at low H_e and coincides with the direction of H_u .¹⁷ In this case, equations for the ac magnetic field in the surface layers can be written in the form

$$\begin{aligned} \frac{d^2 h_y^{(j)}}{dx^2} + \frac{2i}{\delta_0^2} (1 + \mu_2 \sin^2 \varphi) h_y^{(j)} &= \frac{2i}{\delta_0^2} \mu_2 h_z^{(j)} \sin \varphi \cos \varphi, \\ \frac{d^2 h_z^{(j)}}{dx^2} + \frac{2i}{\delta_0^2} (1 + \mu_2 \cos^2 \varphi) h_z^{(j)} &= \frac{2i}{\delta_0^2} \mu_2 h_y^{(j)} \sin \varphi \cos \varphi, \end{aligned} \quad (4)$$

where the superscripts $j=1,2$ correspond to the regions $t/2-t_1 < x < t/2$ and $-t/2 < x < -t/2+t_2$, respectively, and the effective permeability μ_2 of the hard magnetic layers can be presented in the form

$$\begin{aligned} \mu_2 &= \frac{\omega_m(\omega_m + \omega_3 - i\kappa\omega)}{(\omega_m + \omega_3 - i\kappa\omega)(\omega_3 - i\kappa\omega) - \omega^2}, \\ \omega_3 &= \gamma H_u. \end{aligned} \quad (5)$$

The components of the magnetic field at the ribbon surface are determined by the excitation conditions and can be expressed as

$$\begin{aligned} h_y^{(1)} \Big|_{x=t/2} &= 2\pi I(t)/cw, \quad h_z^{(1)} \Big|_{x=t/2} = 0, \\ h_y^{(2)} \Big|_{x=-t/2} &= -2\pi I(t)/cw, \quad h_z^{(2)} \Big|_{x=-t/2} = 0, \end{aligned} \quad (6)$$

where $I(t)$ is the current and w is the ribbon width. Furthermore, the magnetic field should satisfy the continuity conditions at the interfaces between the amorphous region and crystalline layers:

$$\begin{aligned}
h_y^{(a)} \Big|_{x=t/2-t_1} &= h_y^{(1)} \Big|_{x=t/2-t_1}, \quad h_z^{(a)} \Big|_{x=t/2-t_1} = h_z^{(1)} \Big|_{x=t/2-t_1}, \\
h_y^{(a)} \Big|_{x=-t/2+t_2} &= h_y^{(2)} \Big|_{x=-t/2+t_2}, \quad h_z^{(a)} \Big|_{x=-t/2+t_2} = h_z^{(2)} \Big|_{x=-t/2+t_2}, \\
\frac{dh_y^{(a)}}{dx} \Big|_{x=t/2-t_1} &= \frac{dh_y^{(1)}}{dx} \Big|_{x=t/2-t_1}, \quad \frac{dh_z^{(a)}}{dx} \Big|_{x=t/2-t_1} = \frac{dh_z^{(1)}}{dx} \Big|_{x=t/2-t_1}, \\
\frac{dh_y^{(a)}}{dx} \Big|_{x=-t/2+t_2} &= \frac{dh_y^{(2)}}{dx} \Big|_{x=-t/2+t_2}, \quad \frac{dh_z^{(a)}}{dx} \Big|_{x=-t/2+t_2} = \frac{dh_z^{(2)}}{dx} \Big|_{x=-t/2+t_2}.
\end{aligned} \tag{7}$$

The distribution of the magnetic field describing by the set of Eqs. (1) and (4) can be written in the form

$$\begin{aligned}
h_y^{(a)} &= \cos \theta [A_1 \sinh(k_0 x) + A_2 \cosh(k_0 x)] + \sin \theta [A_3 \sinh(k_1 x) + A_4 \cosh(k_1 x)], \\
h_z^{(a)} &= \sin \theta [A_1 \sinh(k_0 x) + A_2 \cosh(k_0 x)] - \cos \theta [A_3 \sinh(k_1 x) + A_4 \cosh(k_1 x)], \\
k_0 &= (1-i)/\delta_0, \quad k_1 = (1-i)(\mu_1 + 1)^{1/2}/\delta_0,
\end{aligned} \tag{8}$$

$$\begin{aligned}
h_y^{(j)} &= \cos \varphi [B_1^{(j)} \sinh(k_0 x) + B_2^{(j)} \cosh(k_0 x)] + \sin \varphi [B_3^{(j)} \sinh(k_2 x) + B_4^{(j)} \cosh(k_2 x)], \\
h_z^{(j)} &= \sin \varphi [B_1^{(j)} \sinh(k_0 x) + B_2^{(j)} \cosh(k_0 x)] - \cos \varphi [B_3^{(j)} \sinh(k_2 x) + B_4^{(j)} \cosh(k_2 x)], \\
k_2 &= (1-i)(\mu_2 + 1)^{1/2}/\delta_0.
\end{aligned} \tag{9}$$

General solution (8) and (9) contains twelve constants, which can be found from Eqs. (6) and (7). After that, the amplitude V_c of the pick-up coil voltage can be calculated as^{11,16}

$$V_c = Z_c I_0 = (2\pi/c) N I_0 \left(\zeta_{yz} \Big|_{x=t/2} + \zeta_{yz} \Big|_{x=-t/2} \right), \tag{10}$$

where N is the number of turns in the pick-up coil and ζ_{yz} is the off-diagonal component of the surface impedance tensor, which can be expressed as^{8,11}

$$\zeta_{yz} \Big|_{\pm x=t/2} = -\frac{c}{4\pi\sigma} \times \frac{dh_z^{(j)}/dx}{h_y^{(j)}} \Big|_{x=\pm t/2}. \tag{11}$$

The calculated field dependence of the off-diagonal magnetoimpedance Z_c is shown in Fig. 4(a) at $f=500$ kHz for different values of the bias field H_b . The values of Z_c are reduced to the dc ribbon resistance $R_{dc}=l/\sigma wt$, where l is the ribbon length. In the model proposed, we assume that the ribbon has a single-domain structure. However, it is well known that at low external fields, a domain structure in the ribbon may exist. In particular, the observed hysteresis of the field dependence of the impedance denotes the appearance of the domain

structure. To calculate the off-diagonal magnetoimpedance, we assume that the stripe domain structure exists at low external fields and average the off-diagonal impedance response over the domain structure. The details of the averaging procedure can be found in Ref. 18. Note also that we assume in calculations that the saturation magnetization, conductivity and damping parameter are the same for the amorphous and crystalline regions. Corresponding modifications taking into account the variations of these parameters can be readily made in the framework of the present approach.

It follows from Fig. 4(a) that the field dependence of the off-diagonal impedance Z_c shows the asymmetric two-peak behavior. The asymmetry grows with the bias field H_b , the negative field peak decreases and the positive field peak increases. The peak values of H_e shift to the direction of the annealing field with the increase of the effective bias field. It is seen from Fig. 4(b) that the asymmetry in the field dependence of the off-diagonal impedance increases with the deviation of the unidirectional anisotropy field from the annealing field direction.

Fig. 5 illustrates the influence of the difference in the thickness of the surface crystalline layers on the off-diagonal magnetoimpedance. It can be easily shown that in the case of the same thickness of the surface layers, $t_1=t_2$, the magnetization distribution is symmetrical with respect to the ribbon center, and the off-diagonal impedance is equal to zero. It follows from Fig. 5 that the off-diagonal impedance Z_c increases with the difference in the surface layers thickness t_1-t_2 , and the field dependence of Z_c remains the same.

The comparison of the calculated field dependence of the off-diagonal impedance with the experimental data is shown in Fig. 2. It follows from Fig. 2 that the calculated dependences are in a qualitative agreement with the experimental results, and the calculated and measured values of the off-diagonal impedance are of the same order of the magnitude. However, some disagreements are clearly seen from Fig. 2. The asymmetry between peaks in the experimental dependences at $f=100$ kHz and $f=500$ kHz is more pronounced as compared with the calculated results. Furthermore, within the region of the negative fields, the measured off-diagonal impedance drops more sharply with the field decrease. These disagreements may be related to the approximations made in the model. In particular, we neglect the coordinate

dependence of the bias field, which allows one to find the solution for the off-diagonal impedance. Taking into account the spatial distribution of the bias field may be essential for a detail description of the asymmetric off-diagonal impedance field dependence. Moreover, to explain the observed hysteresis of the off-diagonal magnetoimpedance, an analysis of the effect of the domain structure should be done. Nevertheless, the approach developed allows one to describe main features of the experimental data.

It should be noted that for the studied field-annealed amorphous ribbons, the impedance response measured as the voltage across the sample changes drastically with the frequency. At low frequencies, the single-peak “GMI valve” has been observed, whereas at high frequencies the GMI profile shows asymmetric two-peak behavior.⁶ The transition from the single-peak to two-peak field dependence of the impedance can be explained as follows.¹⁸ At low frequencies, the main contribution to the permeability is due to the domain-walls motion, and in this case the GMI response has the single-peak behavior. At high frequencies, the domain-walls motion is damped by eddy currents, and the magnetization rotational process determines the permeability, which results in the two-peak GMI profile. On the contrary, the field dependence of the off-diagonal magnetoimpedance shows the two-peak behavior even at low frequencies, since the domain-wall motion contribution to the off-diagonal impedance is sufficiently small.

In conclusion of this section, we assume that the asymmetry in the magnetization distribution over the ribbon thickness is related to the different thickness of the surface crystalline layers, which may be attributed to peculiarities of the field-annealing process. The model allows to one to describe the field dependence of the off-diagonal impedance by using reasonable values of the fitting parameters. Note that the asymmetry may occur also due to other reasons, in particular, due to the variation of the anisotropy field and the anisotropy axis angle over the ribbon thickness. Further investigation of the effect of the annealing conditions on the off-diagonal magnetoimpedance should be performed, and this study is now in progress.

IV. CONCLUSIONS

The results of the study of the off-diagonal magnetoimpedance in the field-annealed Co-based amorphous ribbons are presented. The field dependence of the off-diagonal impedance shows asymmetric two-peak behavior. The asymmetry is related to the formation of the hard magnetic phase due to the surface crystallization of the amorphous ribbons. To explain experimental results, the model based on the concept of the surface impedance tensor is developed. It is assumed that the ribbon consists of the amorphous region and two surface crystalline layers having different thickness. The coupling between the surface crystalline layers and the amorphous phase is described in terms of the effective bias field, which is assumed to be constant over the ribbon volume. The calculated dependences describe qualitatively the experimental data. The results obtained may be useful to develop sensitive magnetic-field sensors.

ACKNOWLEDGMENTS

The authors would like to thank Dr. L. Kraus for fruitful discussions. This work was supported by the Korea Science and Engineering Foundation through ReCamm. N.A.B. acknowledges the support of the Brain Pool Program.

References

¹ L. Kraus, Sensors Actuators A **106**, 187 (2003).

² L. V. Panina, D. P. Makhnovskiy, and K. Mohri, J. Magn. Magn. Mater. **272–276**, 1452 (2004).

³ C. G. Kim, K. J. Jang, H. C. Kim, and S. S. Yoon, J. Appl. Phys. **85**, 5447 (1999).

⁴ K. J. Jang, C. G. Kim, S. S. Yoon, and K. H. Shin, IEEE Trans. Magn. **35**, 3889 (1999).

⁵ Y. W. Rheem, C. G. Kim, C. O. Kim, and S. S. Yoon, J. Appl. Phys. **91**, 7433 (2002).

⁶ C. G. Kim, C. O. Kim, and S. S. Yoon, J. Magn. Magn. Mater. **249**, 293 (2002).

⁷ A. Antonov, I. Iakubov, and A. Lagarkov, IEEE Trans. Magn. **33**, 3367 (1997).

⁸ N. A. Usov, A. S. Antonov, and A. N. Lagar'kov, J. Magn. Magn. Mater. **185**, 159 (1998).

⁹ A. S. Antonov, I. T. Iakubov, and A. N. Lagarkov, J. Magn. Magn. Mater. **187**, 252 (1998).

¹⁰ L. V. Panina, K. Mohri, and D. P. Makhnovskiy, J. Appl. Phys. **85**, 5444 (1999).

¹¹ D. P. Makhnovskiy, L. V. Panina, and D. J. Mapps, Phys. Rev. B **63**, 144424 (2001).

¹² S. Sandacci, D. Makhnovskiy, L. Panina, K. Mohri, and Y. Honkura, IEEE Trans. Magn. **40**, 3505 (2004).

¹³ A. S. Antonov and I. T. Iakubov, J. Phys. D **32**, 1204 (1999).

¹⁴ N. Fry, D. P. Makhnovskiy, L. V. Panina, S. T. Sandacci, D. J. Mapps, and M. Akhter, IEEE Trans. Magn. **40**, 3358 (2004).

¹⁵ D. P. Makhnovskiy, A. S. Antonov, A. N. Lagar'kov, and L. V. Panina, J. Appl. Phys. **84**, 5698 (1998).

¹⁶ L. V. Panina, J. Magn. Magn. Mater. **249**, 278 (2002).

¹⁷ N. A. Buznikov, C. G. Kim, C. O. Kim, and S. S. Yoon, J. Magn. Magn. Mater. **288**, 130 (2005).

¹⁸ N. A. Buznikov, C. G. Kim, C. O. Kim, and S. S. Yoon, Appl. Phys. Lett. **85**, 3507 (2004).

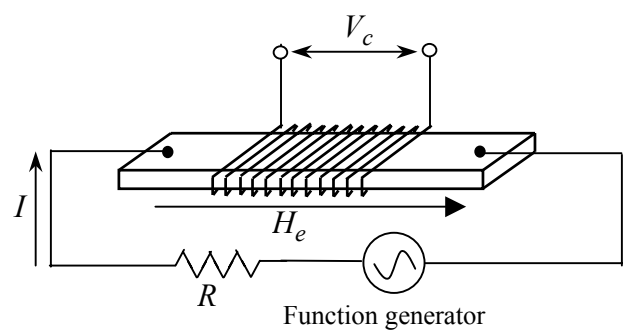


FIG. 1. Schematic diagram of the experimental setup.

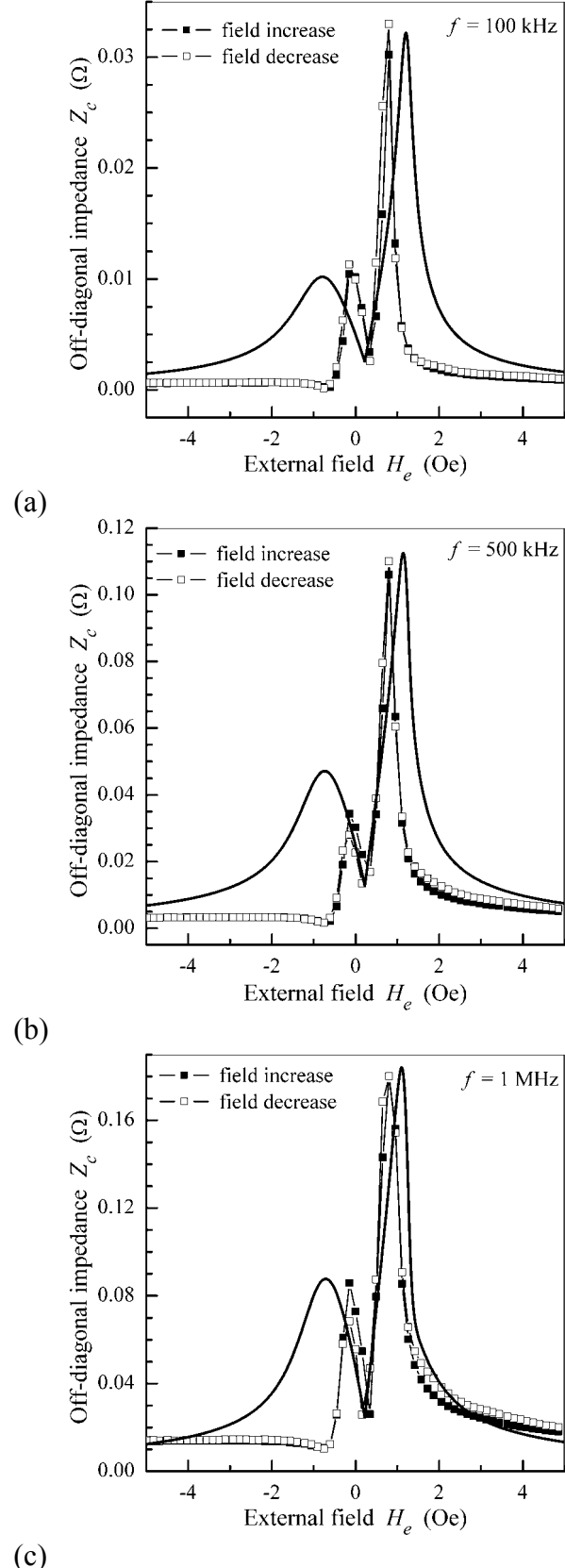


FIG. 2. Dependence of the off-diagonal impedance Z_c on the external field H_e at current frequency $f=100$ kHz (a), $f=500$ kHz (b), and $f=1$ MHz (c). Symbols, experimental data; solid line, calculations. Parameters used for calculations are $M=600$ Gs, $H_a=1$ Oe, $H_u=200$ Oe, $H_b=0.3$ Oe, $\psi=0.05\pi$, $\varphi=0.35\pi$, $\sigma=10^{16}$ s^{-1} , $t_1=1$ μm , $t_2=0.65$ μm , $\kappa=0.1$.

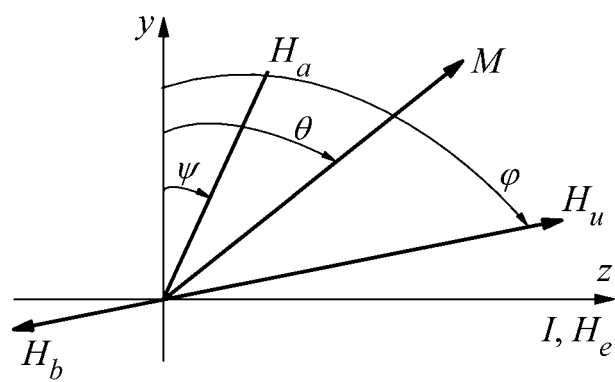


FIG. 3. A sketch of coordinate system used for analysis. All the vectors lie within $y-z$ plane.

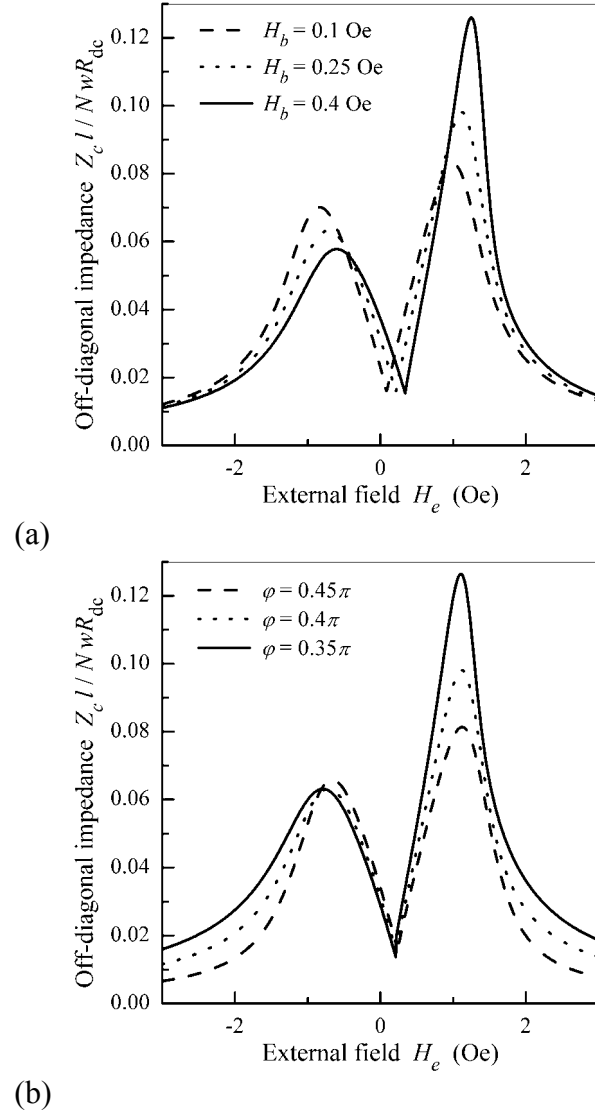


FIG. 4. Off-diagonal impedance Z_c versus external field H_e at $\varphi=0.4\pi$ and different H_b (a) and $H_b=0.25$ Oe and different φ (b). Parameters used for calculations are $M=600$ Gs, $H_a=1$ Oe, $H_u=200$ Oe, $f=500$ kHz, $\psi=0.05\pi$, $\sigma=10^{16}$ s $^{-1}$, $t=20$ μ m, $t_1=1$ μ m, $t_2=0.5$ μ m, $\kappa=0.1$.

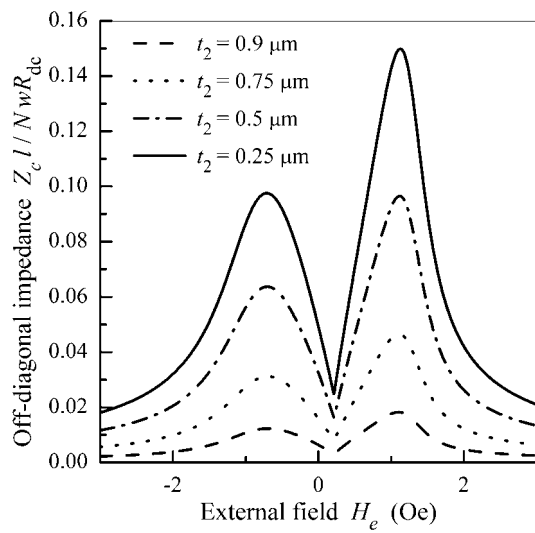


FIG. 5. Off-diagonal impedance Z_c versus external field H_e at $t_1=1\text{ }\mu\text{m}$ and different t_2 . Parameters used for calculations are $M=600\text{ Gs}$, $H_a=1\text{ Oe}$, $H_u=200\text{ Oe}$, $H_b=0.25\text{ Oe}$, $f=500\text{ kHz}$, $\psi=0.05\pi$, $\varphi=0.4\pi$, $\sigma=10^{16}\text{ s}^{-1}$, $t=20\text{ }\mu\text{m}$, $\kappa=0.1$.